Fatigue behaviour of open-hole samples and automotive mini-structures made of woven glass-fibre-reinforced polyamide 6,6

Amélie Malpot[1,*], *Fabienne* Touchard[2], *Sébastien* Bergamo[1], *Catherine* Peyrac[3], *Richard* Montaudon[1], and *Jean-Baptiste* Blumenfeld[1]

[1]Renault SA, 78084 Guyancourt, France
[2]Département Physique et Mécanique des Matériaux, Institut Pprime, 86961 Futuroscope Chasseneuil, France
[3]Pôle Fatigue des Composants Mécanique, CETIM, Senlis, France

Abstract. In the automotive industry, the integration of thermoplastic composite components represents a high-potential solution to the mass reduction challenge. In this study, a woven glass-fibre-reinforced composite with a polyamide 6,6 matrix is considered for the purpose of being integrated into automotive parts. Tension-tension fatigue tests were conducted on $[(0/90)_3]$ open-hole samples. These tests were instrumented with non-destructive techniques, namely acoustic emission and infrared thermography. Acoustic emission results showed fibre-matrix debonding and fibre breakages in open-hole samples, located around the hole. Furthermore, 3-point bending fatigue tests were performed on "omega" mini-structures. A semi-empirical model was used in order to predict the fatigue lives of both open-hole coupons and automotive mini-structures. Predictions of the model for open-holes samples underestimate experimental fatigue lives. Nevertheless, the semi-empirical model showed good results for the fatigue life prediction of composite mini-structures.

1 Introduction

Glass-fibre-reinforced composites with thermoplastic matrix are strategic for automotive manufacturers because of their strength-to-weight ratio, their recyclability, their production rate and their cost. Many vehicle parts are subjected to fatigue loading. The origin of this loading may be the road itself, the users or the engine. Thus, it is important for car manufacturer to be able to predict the fatigue behaviour of composite automotive parts.

According to Degrieck & Van Paepegem [1], fatigue models can be classified in three groups: fatigue life models, phenomenological models to predict residual stiffness/strength and progressive damage models. In the context of this study, fatigue life models seem to be particularly appropriate since they allow the direct determination of the number of cycles at failure for a given set of experimental conditions [2, 3, 4].

Fatigue life model proposed by Epaarachchi & Clausen [4] has been used by several authors in order to model the fatigue behaviour of composite materials. Mortazavian et al. [5] have developed a model based on the work of Epaarachchi & Clausen [4] in order to predict the fatigue life of short-fibre-reinforced polymer. The authors showed that this model is able to predict accurately the fatigue life of short glass fibre/PA66 composite for several temperatures, stress ratios and fibres orientations. Other authors have used the model presented in [4] in order to predict the fatigue life of composite reinforced with continuous fibres [6, 7, 8, 9].

This study is focused on a woven glass-fibre-reinforced polyamide 6,6 (referred as GFRPA66). In a previous study, the influence of fabric orientation and conditioning on fatigue damage of this composite was studied [10]. Moreover, the fatigue life model proposed by [4] was investigated [11]. This model showed a good ability to predict the fatigue lives of the composite material studied for different fabric orientations and conditionings. Thus, the present study is a straight continuation of these studies and tends to evaluate the capacity of this model to predict the fatigue life of open-hole samples and automotive mini-structures.

2 Material and Methods

2.1 Tested material

The composite material studied is made of three plies of a 2/2 twill woven glass fabric impregnated with polyamide 6,6 resin. The glass fibre fabric has a weight of 600 g/m^2 and a warp to weft ratio of 50/ 50. The fibre mass fraction (m_f) is equal to 0.63 and the void content is below 1%. The resulting composite plates are characterised by a density of 1.78 g/cm^3. The material is provided as plates of 1.53 mm thick and coupons are cut using water jet cutting technique. It has been checked

* Corresponding author: amelie.malpot@renault.com

© The Authors, published by EDP Sciences. This is an open access article distributed under the terms of the Creative Commons Attribution License 4.0 (http://creativecommons.org/licenses/by/4.0/).

that this technique has no significant influence on the material moisture content. The specimen edges were polished to remove mechanical damage caused by the cutting.

The glass fibre fabric, referred as $[(0/90)_3]$, has the warp direction of each ply oriented at 0° from the tensile axis (x axis). Polyamide 6,6 being known to be very sensitive to moisture, all samples used in this study were conditioned at RH50.

Mechanical properties of the material are detailed in Table 1.

Table 1. Mechanical properties of $[(0/90)_3]$ GFRPA66 conditionned at RH50

σ_u [MPa]	ε^R [%]	E [GPa]	ν
343.5 ± 1.0	2.05 ± 0.04	17.5 ± 0.5	0.07 ± 0.01

2.1.1 Open-hole samples

Rectangular $[(0/90)_3]$ samples were drilled in the center of the coupon in order to create open-hole samples. The general dimensions of the coupon were 200 x 20 x 1.57 mm. Three diameters were used for the hole, namely 6, 7 and 8 mm.

2.1.2 Mini-structures

Mini-structures studied are shaped by thermoforming of a $[(0/90)_3]$ woven glass-fibre-reinforced polyamide 6,6 plate. The general dimensions of the mini-structure are 730 mm length and 140 mm width. The central part has an omega section (Figure 1).

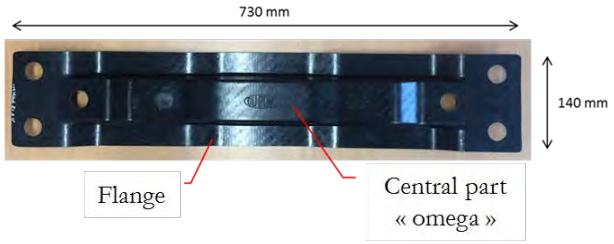

Fig. 1. GFRPA66 mini-structure

2.2 Mechanical testing

Tension-tension fatigue tests on open-hole samples were performed by using an INSTRON 8501 servo-hydraulic machine. The jaws of test machine clamp 40 mm of each specimen extremity and 80 grit sand papers were used in the jaws to improve clamping. Constant amplitude loads were applied in a sinusoidal waveform at the frequency of 1 Hz in order to limit self-generated heating of the specimen. The stress ratio (R), i.e. ratio between minimum (σ_{min}) and maximum (σ_{max}) stresses, was equal to 0.1 for all tests.

3-point bending fatigue tests on mini-structures were performed by using a servo-hydraulic machine, equipped with a 100 kN load cell. Stress ratio is set equal to 0.1 and constant amplitude loads were applied in a sinusoidal waveform at the frequency of 2.5 Hz. The space between the two lower support spans is 480 mm and the span diameter is 30 mm. The load is applied in the middle of the mini-structure using also a 30 mm diameter span.

2.3 Non-destructive techniques and observations

2.3.1 Acoustic Emission (AE)

Acoustic emission monitoring was performed on open-hole samples by using the AE system from Mistras Group. Two sensors Micro-80 with a resonant frequency of 300 kHz and an active surface diameter of 10mm were used. They were placed at the gauge extremities of the specimen using silicon grease as the coupling agent. Sensors are separated with a distance of 100 mm between their centers. The amplitude threshold has been chosen equal to 35 dB. Table 2 shows the settings of the AE system used.

Table 2. Acoustic Emission settings

Preamplifier gain	40 dB
Threshold of detection	35 dB
Type of sensors	Micro-80
Couplant	Silicon grease
PDT (Peak Definition Time)	30 µs
HDT (Hit Definition Time)	100 µs
HLT (Hit Lockout Time)	1000 µs
Resonant Frequency	300 kHz
Bandwidth	1 kHz – 3 MHz

Each test was preceded by a data acquisition calibration step. Using a pencil lead break procedure, the acoustic wave speed as well as the attenuation phenomenon were measured. For the latter, the lead breakage operation was repeated several times between the two sensors, at regular intervals (Hsu-Nielsen method). This procedure has shown that the attenuation phenomenon is negligible in the present work.

Post-processing was done using a multi-parametric identification, based on the k-means algorithm. The k-means algorithm aims to partition observations into k clusters by minimizing the Euclidian distance between each observation and the nearest center ($C_k = c_1, c_2, \ldots, c_k$). This algorithm is unsupervised, which means that the number of clusters k has to be known a priori.
Observations are assimilated to a n-dimensional vector ($X = x_1, x_2, \ldots, x_n$). The k-means algorithm procedure can be detailed as follow:

1. Random initialization of the cluster center for all k-classes ($C_k = c_1, c_2, \ldots, c_k$).
2. Euclidian distance calculation between each observation and cluster centers.

3. Assignment of each observation to the cluster which minimize the Euclidian distance between the observation and the cluster center.
4. Calculation of the new cluster centers for the new k-classes created.
5. Go to step 2 while there is change in the coordinates of the cluster centers.

In this study, observations are acoustic events and n is chosen equal to five among all AE descriptors: amplitude, duration, rise time, energy and number of counts. Each cluster is then associated to one damage mechanism. Studies dealing with woven composite damage process have highlighted three major damage types: matrix cracking, interface damage and fibre breakage [12, 13, 14, 15]. Thus, it was chosen to create three clusters. Attribution of each cluster to one particular damage mechanism was done by using previous results for clustering based on the amplitude only. Several authors [16, 17, 18, 19] have shown that acoustic events with lower amplitudes are associated to matrix cracking whereas those with higher amplitudes are associated to fibre breakage. The intermediate range corresponds to interface damages. Based on these results, each cluster was associated to one damage mechanism depending on its amplitude center value.

2.3.2 Infrared Thermography

An infrared camera from Cedip Infrared Systems with a detector resolution of 90 mm/pixel was used. The energy radiated by the specimen can be converted into temperature levels assuming that the specimen emissivity is known. In this study, this parameter could not be determined experimentally. Thus, instead of the absolute temperature, the temperature variation at the surface of the specimen has been considered.

2.4 Fatigue life model

The fatigue life model used in this study is proposed by Epaarachchi and Clausen [4]. This model allows the prediction of the fatigue life using a very limited amount of experimental data. The model is based on the hypothesis that the material strength undergoes a continuous decay, following a power law as proposed by Caprino and D'Amore [3] (Eq. (1))

$$\frac{d\sigma_N}{dN} = -a \cdot N^{-b} \qquad (1)$$

where σ_N is the residual strength after N cycles, b is a positive definite constant, dependent on the material and the mode of loading, a is assumed to increase linearly with the stress amplitude. Finally, the model is presented in Eq. (2) [4].

$$N_f = \left(1 + \left(\frac{\sigma_u}{\sigma_{\max}}\right) \frac{f^{\beta}}{\alpha(1-R)^{\lambda - R|sin\theta|}} \left(\frac{\sigma_u}{\sigma_{max}}\right)^{\lambda - 1 - R|sin\theta|}\right)^{1/\beta} \qquad (2)$$

where N_f is the fatigue life, σ_{max} is the maximum fatigue stress, σ_u is the ultimate strength, f is the frequency, R is the stress ratio and θ is the smallest angle between the loading axis and the fibres. The parameter λ is assumed to be equal to 1.6 according to Epaarachchi et al. [4].

Hence, α and β are the only two material parameters (dependent on the mode of loading) that need to be determined using experimental data. Only one S-N curve for a given stress ratio, frequency and lay-up is necessary to determine these parameters. In this study, α and β were determined by using the Wöhler curve obtained at RH50 on $[(0/90)_3]$ plain coupons.

3 Results and Discussion

In a previous study [11], the ability of the fatigue model presented in part 2.4 to predict the fatigue life of the GFRPA66 for plain samples with different fibre orientations and conditioning was evaluated. Based exclusively on the Wöhler curve obtained at RH50 on $[(0/90)_3]$ fabric, the model is able to predict correctly the fatigue life of GFRPA66 for any other fabric orientation and conditioning.

For example, Figure 2 shows the fatigue lives determined with this model on $[(\pm45)_3]$ RH100 GFRPA66 plain samples.

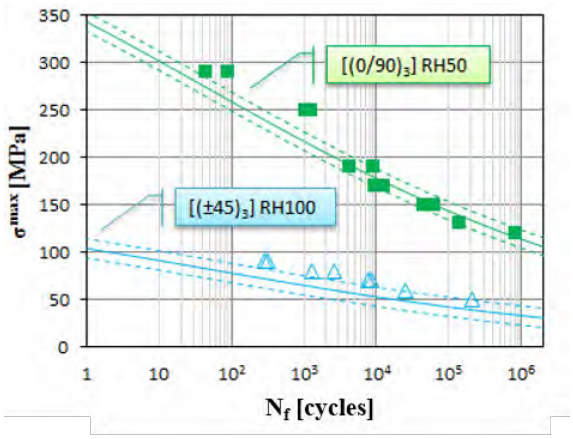

Fig. 2. Experimental (symbols) and estimated (line) fatigue lives of $[(0/90)_3]$ RH50 and $[(\pm45)_3]$ RH100 plain samples (f = 1 Hz, R = 0.1)

This study aims to evaluate the capability of this fatigue life model to predict the fatigue life of open-hole samples and mini-structure.

3.1 Open-hole samples

Monotonic and fatigue tests were conducted on $[(0/90)_3]$ rectangular samples, with a 7 mm diameter hole. Fatigue tests were instrumented with infrared thermography and acoustic emission.

3.1.1 Fatigue life

In first stage, monotonic tensile tests were conducted on open-hole samples at a crosshead speed of 1 mm/min in

order to determine the tensile strength. The stress value is calculated far from the hole and is noted σ_∞.

Fatigue tests were performed in order to determine the fatigue lives of open-hole samples. Results are shown on Figure 3.

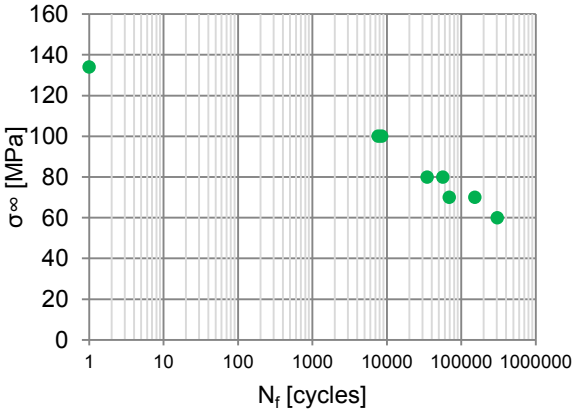

Fig. 3. Experimental fatigue life of $[(0/90)_3]$ open-hole samples (f = 1 Hz, R = 0.1)

In order to apply the fatigue life model (equation 2), it is necessary to determine the local ultimate strength (σ_u) and the maximum local fatigue stress (σ_{max}) around the hole. For that purpose, finite elements simulation was used.

3.1.2 Finite Element Modelling

A simplified FE model (Figure 4) was used by considering that one fabric ply, noted (0/90), is equivalent to the stacking of a 0° UD ply and a 90° UD ply. In order to ensure the symmetry of the stacking, the central woven ply is modelled as the stacking of 4 equivalent UD plies. Finally, the 3 plies $[(0/90)_3]$ woven composite is modelled with the following equivalent UD layup : [0°/90/0°/90°/90°/0°/90°/0°].

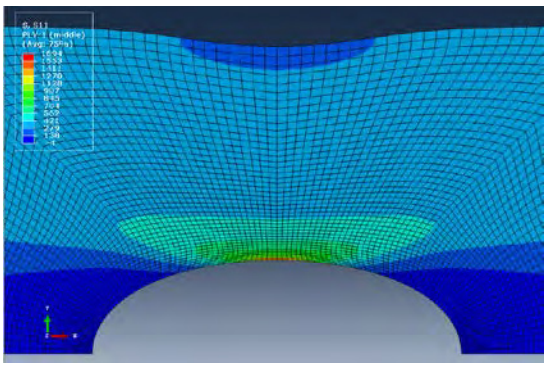

Fig. 4. FE model around the hole (Ø7 mm) of drilled GFRPA66 $[(0/90)_3]$ RH50 specimen.

The elastic coefficients of the equivalent UD plies were determined in order to ensure that the stacking of 0° and 90° plies is equivalent to the woven composite (Table 3).

Table 3. Elastic coefficient of the equivalent UD ply.

E_1 [MPa]	E_2 [MPa]	G_{12} [GPa]	ν_{12}
32800	2200	690	0.33

In order to determine the ultimate local strength around the hole, point stress criterion (PSC) were used. This semi-empirical method states that the material failure occurs when the local stress at a characteristic length (d_0 = 0.42 mm) along the ligament reach the material strength. This characteristic length was determined on 7 mm diameter open-hole samples and then check on 6 mm and 8 mm diameter samples (Table 4).

Table 4. Ultimate local strength for plain material and open-hole samples calculated with PSC method.

	σ_u [MPa]
Plain	344
Ø6	341
Ø7	338
Ø8	339

3.1.3 Fatigue Life Estimation

The model parameters, α and β, are taken equal to those obtained on plain samples. Fatigue life estimation is shown on Figure 5. Results show that the model tends to underestimate the fatigue life of open-hole samples. It is worth noting that the higher the fatigue stress level, the higher the model underestimation. This observation is consistent with the assumption made by Epaarachchi & Clausen [4], i.e. the ultimate strength has to be obtained at the same strain rate as the specimen subjected to fatigue loading. So far, this hypothesis was not taken into account since monotonic tensile tests were performed at 1 mm/min.

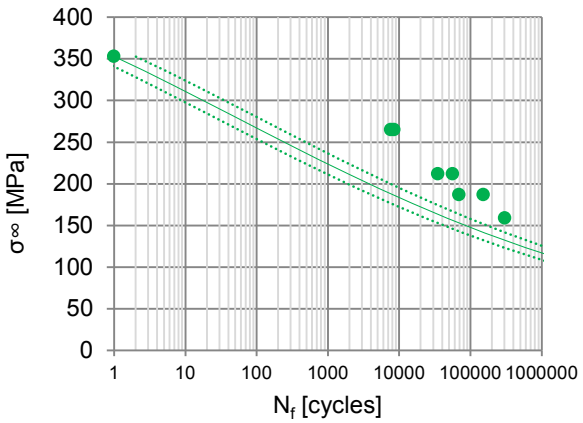

Fig. 5. Fatigue life estimation of open-hole samples (f = 1 Hz, R = 0.1)

3.1.4 Damage evolution

Fatigue tests on open-hole samples were instrumented with infrared thermography and acoustic emission. Figure 6 shows the surface temperature variation observed at the end of a fatigue test.

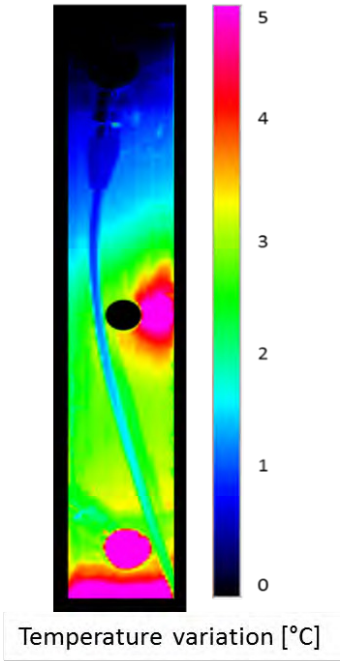

Fig. 6. Temperature variation at the end of a fatigue test.

Figure 6 shows a localized heating of the coupon on the right side of the hole indicating a damage initiation on the edge of the hole.

This observation was confirmed by acoustic emission results (Figure 7). Results show an accumulation of events related to interface and fibre damage around the hole (position = 100 mm). Meanwhile, matrix damage is recorded in the entire coupon.

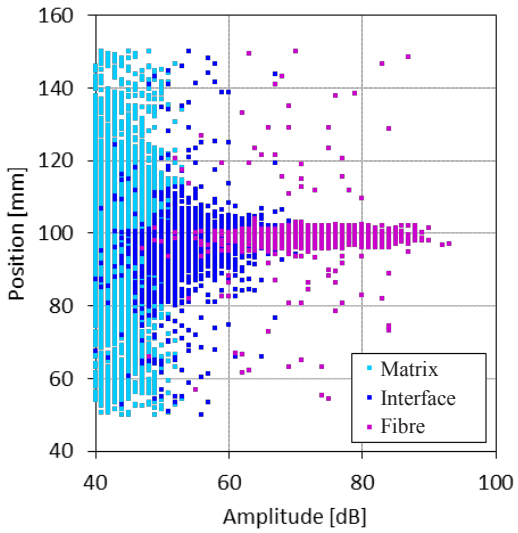

Fig. 7. Acoustic events location recorded during a fatigue test conducted on open-hole sample.

3.2 Automotive mini-structures

3.2.1 Monotonic 3-point bending

GFRPA66 mini-structures were studied in 3-point bending. First, monotonic tests were conducted at a speed of 3 mm/min. Force vs. span displacement curve is shown on Figure 8.

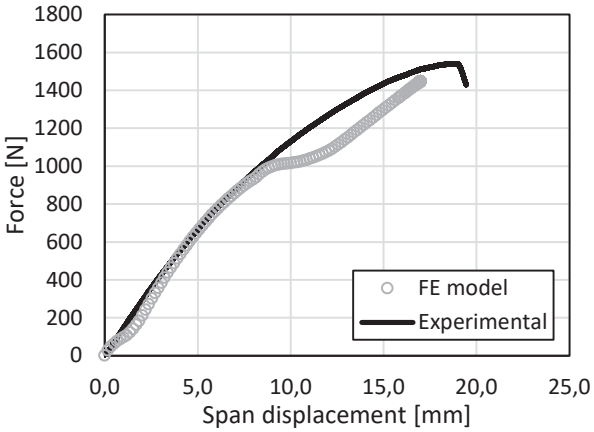

Fig. 8. Numerical and experimental force vs. span displacement curves.

A FE model was developed in order to simulate the behavior of the mini-structure (Figure 9). The woven GFRPA66 material was modelled by the equivalent UD layup [0°/90/0°/90°/90°/0°/90°/0°].

Figure 8 shows the force vs. span displacement curve obtained with FE model. The numerical model shows a good fitting to experimental data until 1000 N. Beyond, some geometrical effects appear in the FE modelling leading to a deviation from the experimental data.

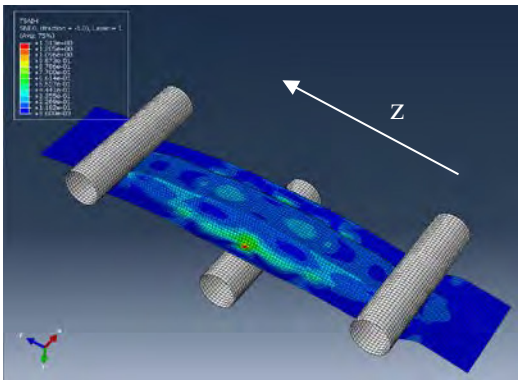

Fig. 9. FE model of the mini-structure.

3.2.2 3-point bending fatigue

Fatigue tests were performed on automotive mini-structures at three force levels. The experimental fatigue lives are shown on Figure 10.

A preliminary study was done by applying the fatigue life model with force instead of stress. For the force-based version of the model, the tensile strength (σ_u) and the maximum fatigue stress (σ_{max}) were respectively replaced by the force at failure and the maximum fatigue force. Moreover, the model parameters α and β being dependent of the loading mode, 3-point bending fatigue tests were conducted on rectangular coupons in order to determine a new set of parameter. The estimated fatigue life of the composite mini-structure are shown on Figure 10 together with experimental data.

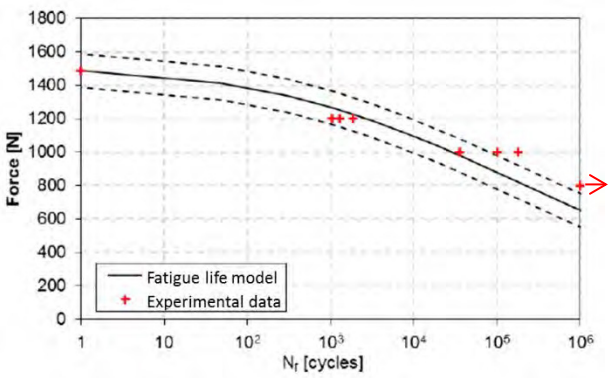

Fig. 10. Experimental and estimated fatigue life of the GFRPA66 mini-structure with the force-based model.

This preliminary version of the model gives satisfactory results in terms of fatigue life estimation. However, it can be improved in order to be applied in an industrial context.

In order to use the semi-empirical model as it is given in equation 2, a representative local stress has to be chosen. In a first stage, the maximum local stress in the z direction (as given in Figure 9) has been chosen. The FE model was used in order to determine this local stress value (noted σ_{zz}) for the different maximum force levels used in fatigue tests and for the force at failure.

Then, the model presented in equation 2 was applied with the set of parameter determined for 3-point bending. Results are shown on Figure 11. The model gives a very good fitting to experimental data, proving its ability to be used in order to evaluate the fatigue life of a composite mini-structure.

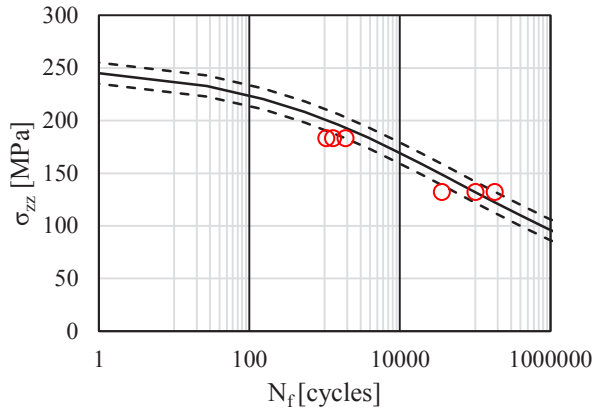

Fig. 11. Experimental and estimated fatigue life of the GFRPA66 mini-structure with the stress-based model.

Additional fatigue tests on mini-structures with a different fabric orientation, $[(\pm 45)_3]$ for instance, could be used in order to validate the semi-empirical model for a different fibre orientation. This could also validate the initial choice of using the local stress in the z direction.

4 Conclusions

This study deals with the fatigue behavior of a woven glass-fibre-reinforced composite with PA66 matrix. Tension-tension fatigue tests were performed on open-hole samples. These tests were instrumented with acoustic emission and infrared thermography. Monitored data have highlighted a damage accumulation around the hole, identified as fibre-matrix debonding and fibre breakages. A fatigue life model was applied on open-hole sample, with material parameters determined on plain samples. Results show a slight underestimation of the fatigue life.

In addition, 3-point bending fatigue tests were performed on automotive mini-structures. The fatigue life model tested on open-hole samples were also applied on mini-structure. As a reminder, the inputs needed for the use of this model are:

- A Wöhler curve obtained on rectangular samples tested in 3-point bending ;
- A numerical model of the mini-structure ;
- A monotonic 3-point bending test for the validation of the numerical model ;

With these data, it is then possible to estimate the fatigue life of the mini-structure in 3-point bending mode. Estimated fatigue lives of the mini-structure were very close to those obtained experimentally, indicating a good capacity of this model to predict the fatigue life of GFRPA66 mini-structure.

References

1. J. Degrieck, W. Van Paepegem. Appl. Mech. Rev., **54**(4), 279-300 (2001)
2. R. Sarfaraz, A.P. Vassilopoulos, T. Keller. Compos. Part A Appl. Sci. Manuf. **43**(3), 445-453 (2012)
3. G. Caprino, A. D'Amore. Compos. Sci Technol, 58(97), 957-965 (1998)
4. J.A. Epaarachchi, P.D. Clausen, Compos. Part A Appl. Sci. Manuf. **34**, 313–326 (2003)
5. S. Mortazavian, A. Fatemi, Int. J. Fatigue, **77**, 12–27 (2015)
6. C. Colombo, F. Libonati, A. Salerno, L. Vergani. Procedia Eng. **10**, 3518–3527 (2011)
7. M.R. Satapathy, B.G. Vinayak, K. Jayaprakash, N.K. Naik, Mater. Des. **51**, 347–356 (2013)
8. R. Ben Toumi, J. Renard,M. Monin, P. Nimdum. Procedia Eng. **66,** 723–736 (2013)
9. D.S. de Vasconcellos, F. Touchard, L. Chocinski-Arnault. Int. J. Fatigue **59,** 159–169 (2014)
10. A. Malpot, F. Touchard, S. Bergamo. Compos. Part B **130,** 11-20 (2017)
11. A. Malpot, F. Touchard, S. Bergamo. Mater. Des. **98**, 12-19 (2016)
12. T. Fujii , S. Amijima, K. Okubo. Compos Sci Technol **49**, 327-333 (1993)
13. S.D. Pandita, G. Huysmans, M. Wevers, I. Verpoest. Compos Part A Appl Sci Manuf **32**, 1533 – 1539 (2001)
14. S. Daggumati, I. De Baere, W. Van Paepegem, J. Degrieck,J. Xu, S.V. Lomov, et al. Compos Sci Technol, **70,** 1926 - 1933 (2010)

15. T. Osada, M. Mizoguchi, M. Kotaki. ICCM13, Beijing (China) (2001)
16. S. Barré, M.L. Benzeggagh. Compos Sci Technol, **3538**, 369 – 376 (1994)
17. D. Scida, Z. Aboura, M.L. Benzeggagh. Compos Sci Technol, **62**, 551 – 557, (2002)
18. D. Silva de Vasconcellos. Thèse, ENSMA, 2013.
19. G. Kotsikos, J.T. Evans, A.G. Gibson, J. Hale. Polym Compos, **20**, 689 - 696 (1999)